JOURNAL OF MATERIALS SCIENCE 29 (1994) 1101–1108

Cavitation erosion of aluminium alloys

W. J. TOMLINSON, S. J. MATTHEWS*
Department of Materials, Coventry University, Coventry, CV1 5FB, UK

Cast aluminium–silicon, cast aluminium–zinc and mechanically alloyed aluminium alloys were eroded in distilled water using a 20 kHz ultrasonic vibratory device. The erosion was measured by weight loss, and the damaged surface was examined using metallographic and profilometric techniques. The maximum differences in the incubation period, in the linear erosion rate and in the mass loss after a 10 h exposure for the nine materials investigated were 620%, 740% and 250%, respectively. The mechanically alloyed materials had by far the best combination of erosion properties. The cast Al–Si alloys had the poorest resistance to erosion. Age hardening was particularly beneficial with the Al–Si alloy. The main mechanism of material removal in all the alloys is by plastic deformation and ductile fracture.

1. Introduction

Cavitation is the growth and collapse of bubbles due to local pressure fluctuations in a liquid [1]. This collapse is accompanied by a sudden flow of liquid which may generate a stress pulse ranging from a few hundred to 1000 MPa [2], and the rapid repetition of the stress, on nearby solids, erodes the surface material by a process that has been likened to shock fatigue [1, 3]. Recent work has shown that good correlations exist between material-removal rates and cyclic-deformation parameters, and this is taken to be a strong indication that damage in cavitation erosion is basically a fatigue process [4]. In general, there are only two ways that the extent of cavitation erosion damage may be reduced: by the design of hydrodynamic profiles, and by the use of erosion-resistant materials [1].

Aluminium is one of the least erosion-resistant materials (see for example the data in [4]), and it has frequently been used to study the early stages and mechanism of cavitation damage [5–8]. Aluminium alloys have a wide range of properties from the relatively weak, commercially pure aluminium to the high-strength aluminium–zinc alloys. The cavitation erosion of the Al–Cu, Al–Mg and Al–Zn–Mg–Cu alloys have been investigated in detail [9–12]. Vaidya and Preece [9] observed that for a number of age-hardening alloys the mechanism of erosion depended strongly on the microstructure. In the dilute alloys, extensive plastic deformation and ductile fracture occurred evenly over the surface. As the concentration of the alloy elements increased (by a few percent), there was a gradual change in the mechanism of damage until the surface was covered with large pits. The fracture surface of the pits in the more concentrated alloys had fatigue-like striations. Alloys with the highest concentration of alloying elements (about 10%), had a quite different erosion behaviour: the amount of surface deformation was small and the pits were of a microscopic size.

A particular problem that occurred in the past, was the cavitation erosion of cast aluminium–silicon alloy rotors and stators in hydrokinetic brakes using a water/glycol mixture [13]. However, there have been no studies on the cavitation erosion behaviour of these and other alloys, and the present work investigated the cavitation erosion of a low-alloyed aluminium, and various commercial Al–Si, Al–Zn and mechanically alloyed alloys.

2. Experimental procedure

A range of materials covering a low-alloyed aluminium, various casting alloys and two mechanically alloyed materials were investigated, and the main details, suppliers, and properties are given in Table I. The low-alloyed aluminium contained about 2.5% solute (Si,Mg,Mn) and had a high ductility and uniform microstructure. It was included as a standard for the test procedure and as a comparison for the other alloys. The major feature of the Al–Si alloys was the interdendritic network of coarse intermetallic compounds. The Al–Zn alloys were gravity die cast and tested in the as-cast (AC) condition, in the solution-treated and artificially aged (T6) condition and in the solution-treated and stabilized (T7) condition.

Mechanically alloyed (MA) alloys are new materials with excellent mechanical properties due to a fine dispersion of aluminium oxide and carbide particles in a very fine microstructure. Microstructures of the materials are illustrated later in the presentation of eroded surfaces.

An anvil erosion-testing arrangement was used (see, for example [3]). The specimen was firmly attached in a rigid stainless-steel jig attached to the body of a 20 kHz ultrasonic device (type S3820, Sonic Systems

Present address: British Gas plc, Gas Research Centre, Ashby Road, Loughborough, LE11 3QU, UK.

0022–2461

TABLE I Material properties

Material designation[a]	Specification	Metallurgical condition	Microstructure[b]	Microhardness (HV 0.2)[c]	0.2% yield stress[d] (MPa)
Al	AL6082	Extruded	Fine dispersion of intermetallics	115	–
Al7Si–AC	LM25	Cast	Intermetallic network	54	–
Al7Si–T6	LM25	Age hardened	Intermetallic network	104	–
Al11Si–AC	LM13	Cast	Intermetallic network	86	–
AlZn–AC	AL7049	Cast	Elongated grains and fine dispersoids	212	–
AlZn–T6	AL7049	Age hardened	Elongated grains and fine dispersoids	213	–
AlZn–T7	AL7049	Solution treated and stabilized	Elongated grains and fine dispersoids	211	–
AlMg–MA	AL9052	Extruded	Fine dispersoids in a very-fine-grain matrix	144	380
AlMgLi–MA	AL905XL	Extruded	Fine dispersoids in a very-fine-grain matrix	145	448

[a] Suppliers: Al, Philip James Engineering Ltd, Coventry; Al7Si, Milver Metal Co., Coventry; Al11Si, ICI plc, Runcorn; AlZn, Royal Ordnance plc, Westcott; MA, Inco Alloys Ltd., Hereford, UK.
[b] For the main features, see the text.
[c] An average of six measurements of the microhardness of the matrix.
[d] From Inco Alloys International Ltd, Hereford, UK (see[a]).

Ltd, Taunton). The erosion fluid was a fresh charge of 800 ml of distilled water in a 2 l polypropylene beaker held in a water bath. The temperature of the water was maintained at 18 ± 1 °C during testing.

The operating conditions were: horn peak-to-peak amplitude 50 ± 2 μm, horn-tip immersed 3–6 mm in the water, sample surface 1 ± 0.1 mm from the horn tip, and the specimen at least 5 mm thick with a surface finish of 1 μm. Full details of the apparatus, calibration, materials, and the effects of horn–sample separation, and the surface finish on the erosion kinetics, have been given elsewhere [14].

The erosion was measured by mass loss using a chemical balance accurate to 0.1 mg. Three series of experiments were conducted on separate specimens. A specimen was weighed every 30 s until a weight loss of 0.1 mg was detected, and the total time taken was defined as the incubation period. Erosion kinetics for up to 3 h exposure were obtained by weighing the specimen every 15 min for the first hour and thereafter every 30 min. Samples tested for 10 h were reweighed, as above, for up to 3 h exposure, and then every hour. Standard metallographic and profilometric techniques were used to examine and measure the eroded surfaces. All microhardness results were for an average of six measurements.

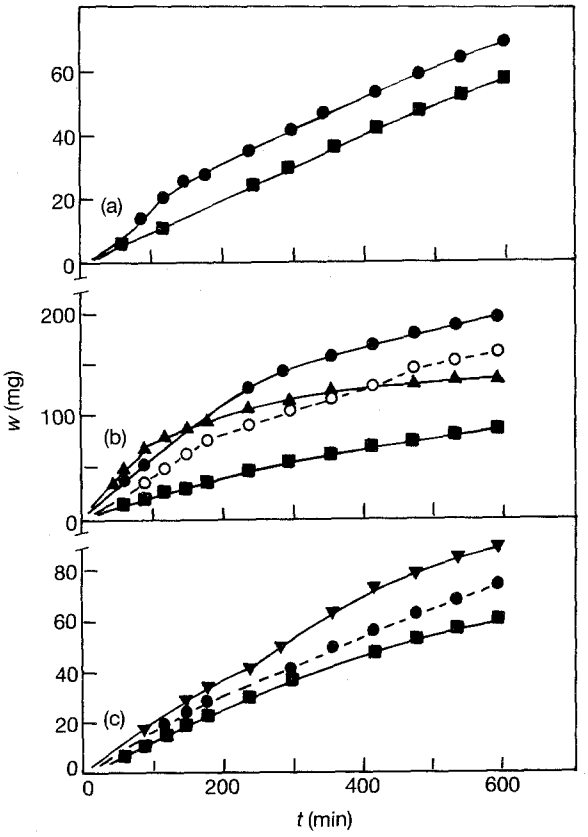

Figure 1 Mass loss, w, as a function of time, t, for various aluminium alloys eroded in distilled water. Some points near the origin have been omitted for clarity. (a) (●) AlMg–MA, and (■) AlMgLi–MA; (b) (○) Al, (●) Al7Si–AC, (■) Al7Si–T6, and (▲) Al11Si–AC; (c) (●) AlZn–AC, (■) AlZn–T6, and (▼) AlZn–T7.

3. Results

The erosion behaviour for each of the materials is shown in Fig. 1. A uniform pattern of erosion kinetics occurs. In each case there is an incubation period where no, or less than 0.1 mg loss of material, occurs, followed by a period of accelerating erosion which leads to a linear erosion rate. The linear erosion rate is also the maximum erosion rate, and after further exposure to cavitation there is a steady decrease in the erosion rate (Fig. 1). The final decrease in erosion can be considerable; for example, the final erosion rate of the Al11Si–AC alloy was only 3% of the maximum

erosion rate. Full details of the erosion results and parameters are given in Table II. The incubation period was measured by weighing a specimen every 30 s until a weight loss of 0.1 mg was observed. Duplicate tests were used to obtain graphs (not illustrated), and from these graphs the linear erosion rates and the extrapolation of the linear rate to the time axis intercept were obtained. For convenience, the ratios of the incubation period of the alloy to that of low-alloyed aluminium, and of the average linear erosion rate of the alloy to that of low-alloyed aluminium, are also given in Table II.

There is a large amount of information in Table II. Overall, it can be seen that there is a wide variation in the value of a parameter from one material to another. Thus the differences between the maximum and minimum values of the incubation period, the linear erosion rate and the weight loss after 10 h were 620%, 740% and 250%, respectively. The most important feature of the results is the outstanding cavitation erosion resistance of the mechanically alloyed materials, which have an excellent reproducibility, and the combination of by far the longest incubation period with one of the lowest erosion rates measured in terms of either the linear rate or the total weight loss. The aluminium–zinc materials also have a low erosion rate, but unlike the mechanically alloyed materials, this is combined with a short incubation period. The aluminium–silicon alloys have the least resistance to erosion. Age hardening has a substantial effect on the cavitation erosion resistance of the Al7Si–AC material. It increases the incubation period by 300% and decreases the linear rate by 50%.

Eroded specimens were examined macroscopically at the end of the incubation period and after 3 h and 10 h erosion. Two photographs are shown in Fig. 2. In all the specimens, the surface was finely and uniformly deformed with many fine pits (Fig. 2a) at the end of the incubation period. After 3 h and 10 h erosion, the surface was very rough with deep pits and craters. The Al–Zn alloy was unusual inasmuch as the erosion occurred preferentially on certain planes, and this effectively etched the cast grain microstructure (Fig. 2b).

Metallographic sections of each of the alloys, at the end of the incubation period and after 3 and 10 h erosion, were examined; representative features are shown in Figs 3–5. A similar pattern of behaviour occurred in the Al, AlMg–MA, and AlMgLi–MA materials, see Fig. 3, for example. The surface was roughened in the incubation period (Fig. 3a). After 3 h erosion, large craters formed which were about 500 μm wide and 250 μm deep in the Al, and 100 μm wide and 50 μm deep in the MA alloys, many fine cracks also formed (Fig. 3b). The craters later joined to give a very roughened surface with cracks up to 30 μm deep (Fig. 3c).

Deformation and roughness was far less in the Al–Si alloys, and there was a tendency for the intermetallic compounds to be preferentially removed (Fig. 4). The compounds generally influenced the formation of cracks near the surface, particularly where the interdendritic regions were normal to the surface. Once the thickness of the damaged layer was appreciable, there was a tendency for the cracks to be parallel to the surface and to be relatively uninfluenced by the intermetallic network (Figs 4b and c).

In contrast to the other materials, all the Al–Zn materials showed only extremely light deformation in the incubation period, and thereafter generally local-

TABLE II Erosion results and parameters

Material	Incubation period, I_P (min)	Ratio $\left(\frac{I_P\ (\text{alloy})}{I_P\ (\text{Al})}\right)$	Nominal incubation period[a] (min)	Weight loss[b]		Erosion rate[b] (mg h^{-1})	Average erosion rate, r (mg h^{-1})	Ratio $\left(\frac{r(\text{alloy})}{r(\text{Al})}\right)$
				3 h (mg)	10 h (mg)			
Al	9	1.0	27	76.0	162.2	30.0	30.6	1.0
				71.7		31.2		
Al7Si–AC	2.5	0.3	7	97.1	196.3	41.5	37.4	1.2
				89.7		33.2		
Al7Si–T6	7	0.8	17	41.0	86.6	19.9	18.8	0.6
				34.3		15.2		
				37.8		19.1		
Al11Si–AC	2.5	0.3	16	86.4[c]	136.7	66.2	63.3	2.1
				84.7[c]		60.4		
AlZn–AC	6	0.7	5.5	28.4	73.2	9.7	9.3	0.3
				25.5		8.8		
AlZn–T6	4	0.4	9	22.4	59.4	7.9	7.5	0.2
				21.1		7.1		
AlZn–T7	4	0.4	2.5	34.0	87.4	11.3	12.5	0.4
				41.3		13.6		
AlMg–MA	15	1.7	24	29.2	67.9	12.6	12.6	0.4
				27.1		12.6		
AlMgLi–MA	18	2.0	31	21.9	56.8	8.4	8.4	0.3
				19.7		8.4		

[a] Intercept of the erosion rate with the time axis.
[b] Duplicate tests for exposure up to 3 h. From each of these tests the steady state (maximum erosion rate) was determined. Only one run was continued for 10 h.
[c] The test ran for 2.5 h.

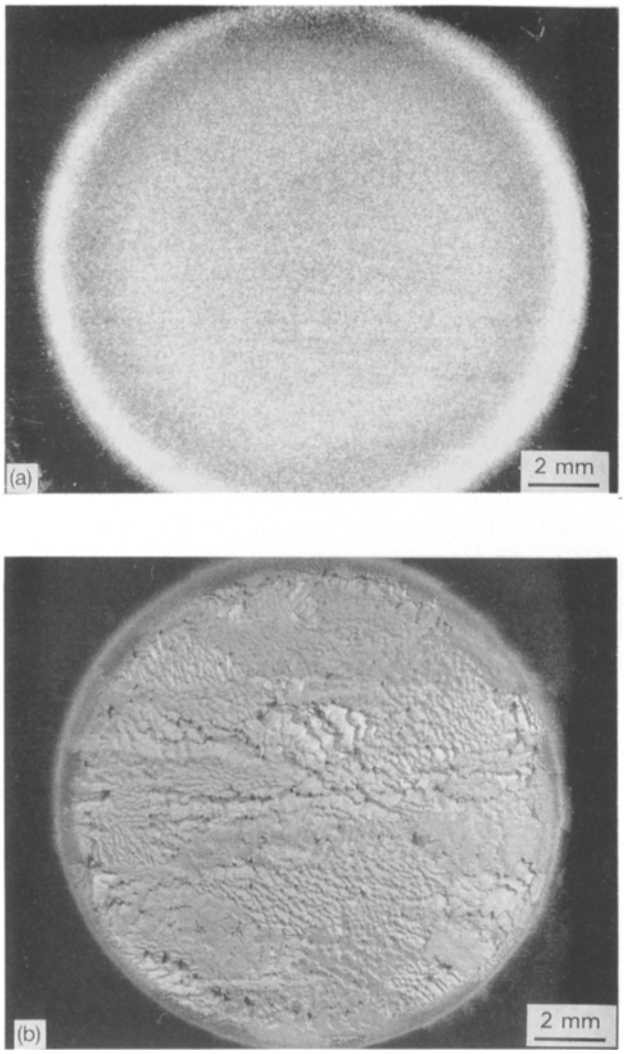

Figure 2 The surface of the AlZn–AC alloy after erosion for: (a) 6 min (incubation period), and (b) 10 h.

ized plastic deformation (Fig. 5). After 3 h erosion, there were broad, largely flat-bottomed craters about 50 μm deep, and many cracks 2–5 μm long parallel to the surface. Further deformation formed pits nearly 200 μm deep with cracks up to 100 μm long (Fig. 5c).

When the surface roughness during the incubation period was sufficiently small, it was possible to obtain a microhardness reading on the exposed surface. Not all the materials were examined in this way, and the results obtained are shown in Fig. 6. It can be seen that a uniform increase in the hardness and work hardening occurs during the early stages of erosion. The microhardness of all the alloys were also measured on sections just below the surface after erosion for the incubation period, 3 h, and 10 h, and also at depths of 250 μm and 500 μm below the surface. In contrast to the hardness on the surface (Fig. 6), the hardnesses in these sections (not illustrated) did not show any regular pattern with respect to either the erosion time or the depth below the surface.

All the materials were examined on the eroded surface at intervals in the incubation period, and beyond, to determine the origin and evolution of the surface damage. For example, the Al11Si–AC material was examined after polishing and after erosion for

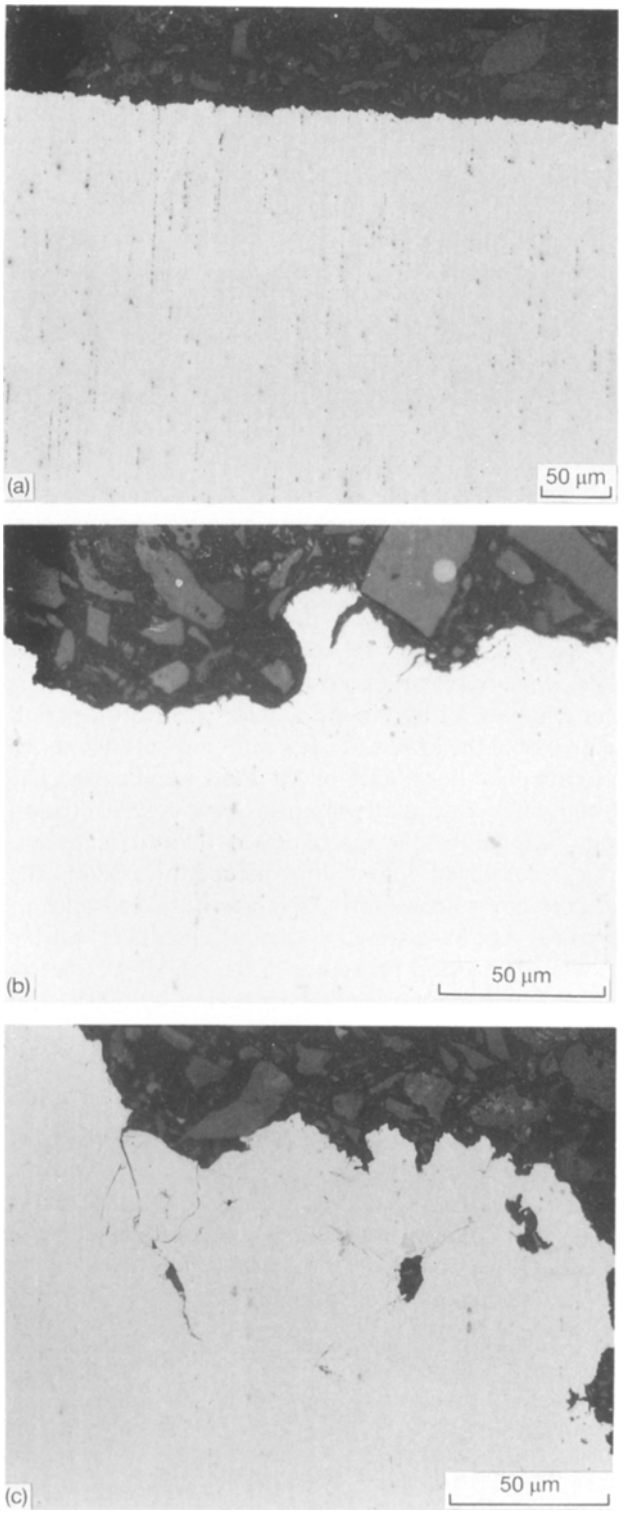

Figure 3 Sections of eroded surface of the AlMg–MA alloy after various times: (a) incubation period (15 min), (b) 3 h, and (c) 10 h.

10 s, 30 s, 1 min and 10 min. Selected photographs are shown in Fig. 7. In Fig. 7a, the intermetallic compounds and shrinkage porosity are clearly visible. Deformation of the matrix closed the porosity (Fig. 7b). After 1 min erosion, considerable distortion of the matrix occurred, leaving the intermetallic compounds apparently unaffected (Fig. 7c). Continued deformation of the matrix leads to necking and rupture of the surface layers, and undermining and detachment of the intermetallics (Fig. 7d). All the

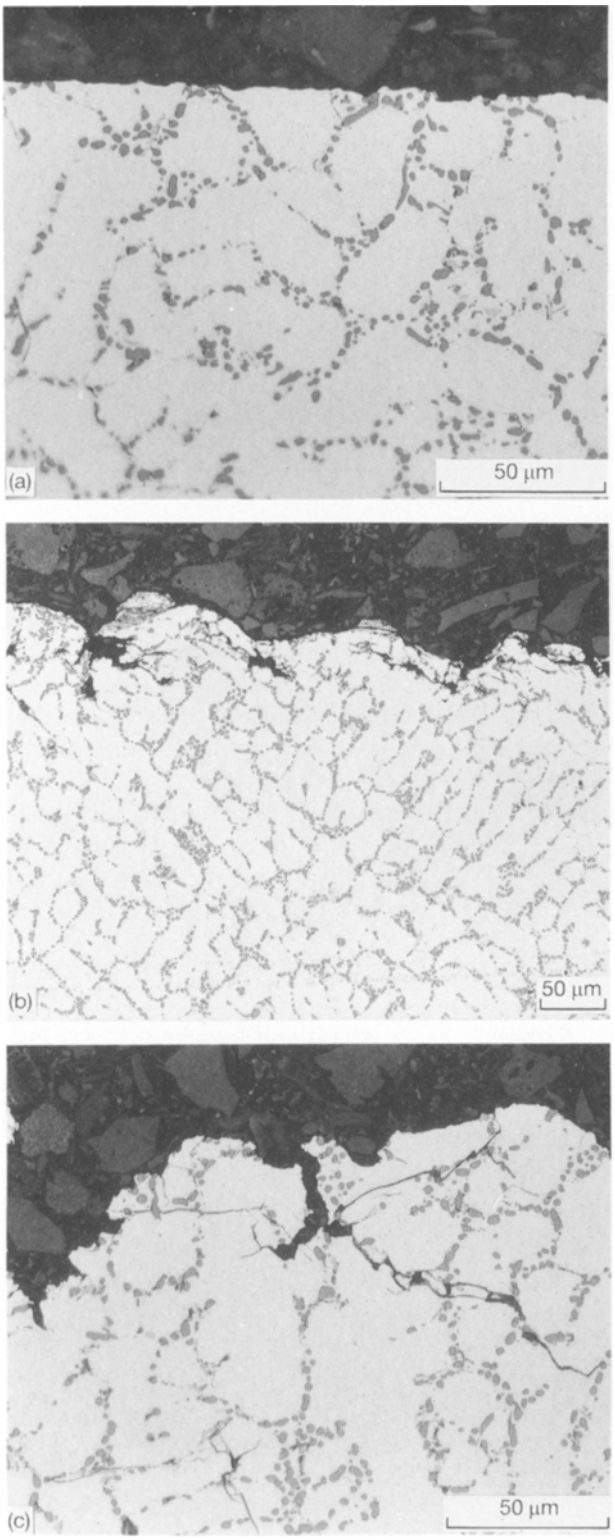

Figure 4 Sections of the eroded surface of the Al7Si–T6 alloy after various times: (a) incubation period (7 min), (b) 3 h, and (c) 10 h.

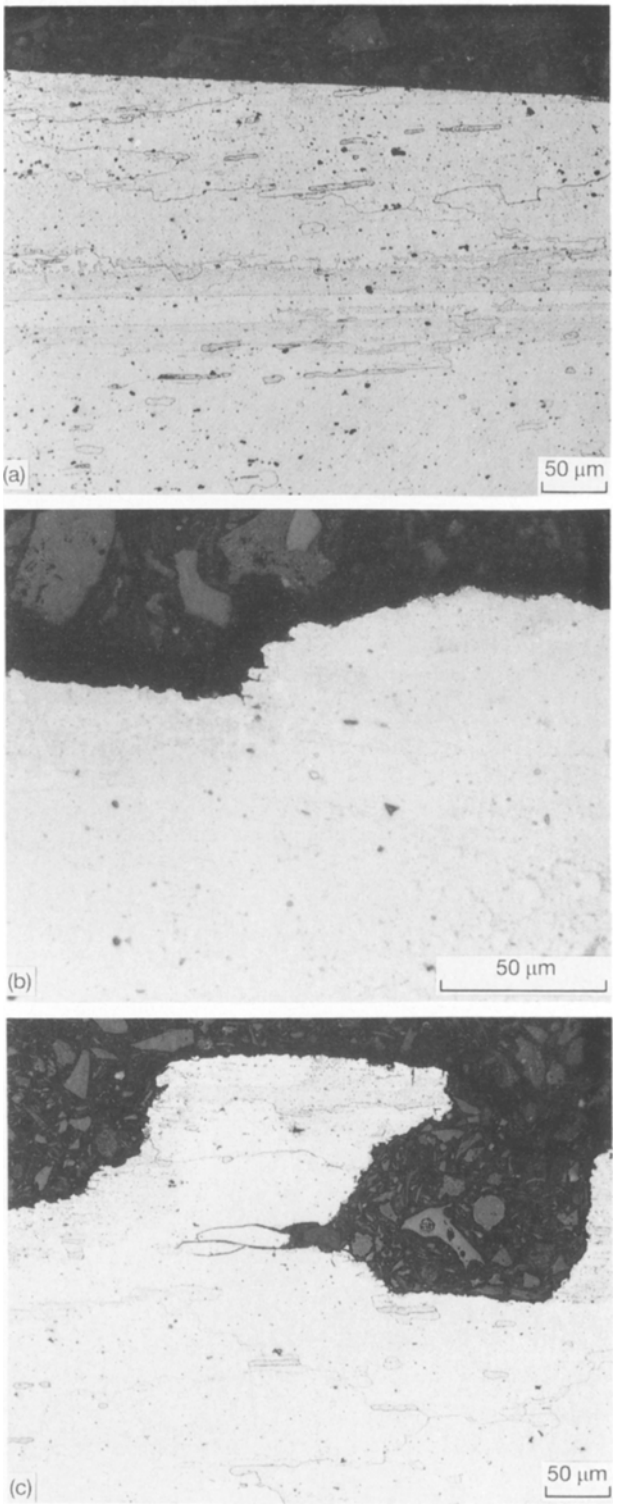

Figure 5 Sections of eroded surface of the AlZn–AC alloy after various times: (a) incubation period (6 min), (b) 3 h, and (c) 10 h.

materials followed a broadly similar pattern of behaviour, but with two significant differences. First, the finely dispersed phases in the mechanically alloyed materials strengthened the matrix; this clearly resisted the deformation, the onset of pitting and the breakdown of the surface (Fig. 8a), and it promoted a smaller scale of deformation (Fig. 8b). Secondly, in the Al–Zn alloys, the bottom of the pits had fatigue-like striations (Fig. 9).

Roughness parameters at the end of the incubation period are given in Table III. It is seen that materials that had a small dispersed phase (Al, AlMg–MA, AlMgLi–MA) had the roughest surfaces, whereas the cast materials (Al7Si–AC is an exception) had a smoother surface. The negative skew indicates a pitted surface [15]. The Al11Si–AC material with a positive skew is unusual. This indicates that the material has a lumpy surface rather than one that is pitted. We may

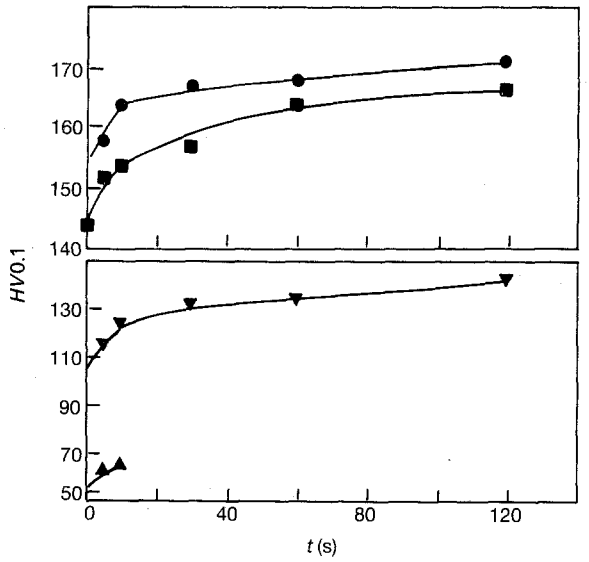

Figure 6 Microhardness, $HV\,0.1$ of the exposed eroded surface as a function of time, t. (●) AlMg–MA, (■) AlMgLi–MA, (▲) Al7Si–AC, and (▼) Al7Si–T6.

also note that a Gaussian surface has Sk = 0 and Ku = 3 [15], and hence on the basis of Sk and Ku values the Al and mechanically alloyed materials appear to have a more regular deformation behaviour than the cast alloys.

TABLE III Roughness parameters at the end of the measured incubation period

Material	Roughness		
	Ra[a] (μm)	Sk[b]	Ku[c]
Al	2.21	− 0.4	2.9
Al7Si–AC	1.66	− 0.2	2.6
Al7Si–T6	0.66	− 1.1	6.3
Al11Si–AC	0.84	+ 1.2	6.0
AlZn–AC	0.38	− 0.4	3.2
AlZn–T6	0.35	− 1.1	4.9
AlZn–T7	0.35	− 1.3	6.2
AlMg–MA	1.39	− 0.1	3.0
AlMgLi–MA	1.41	− 0.5	3.6

[a] Ra = root mean square.
[b] Sk = skewness.
[c] Ku = kurtosis.

Debris collected after erosion for 10 h for each material was collected and examined by scanning electron microscopy (SEM). In each case (not illustrated) there was a range of particle sizes. The largest particles, 200–300 μm, occurred in debris from the Al, Al7Si–AC and Al11Si–AC materials. The other materials had particles with a maximum size of about 50 μm. The particles were always very irregular in shape.

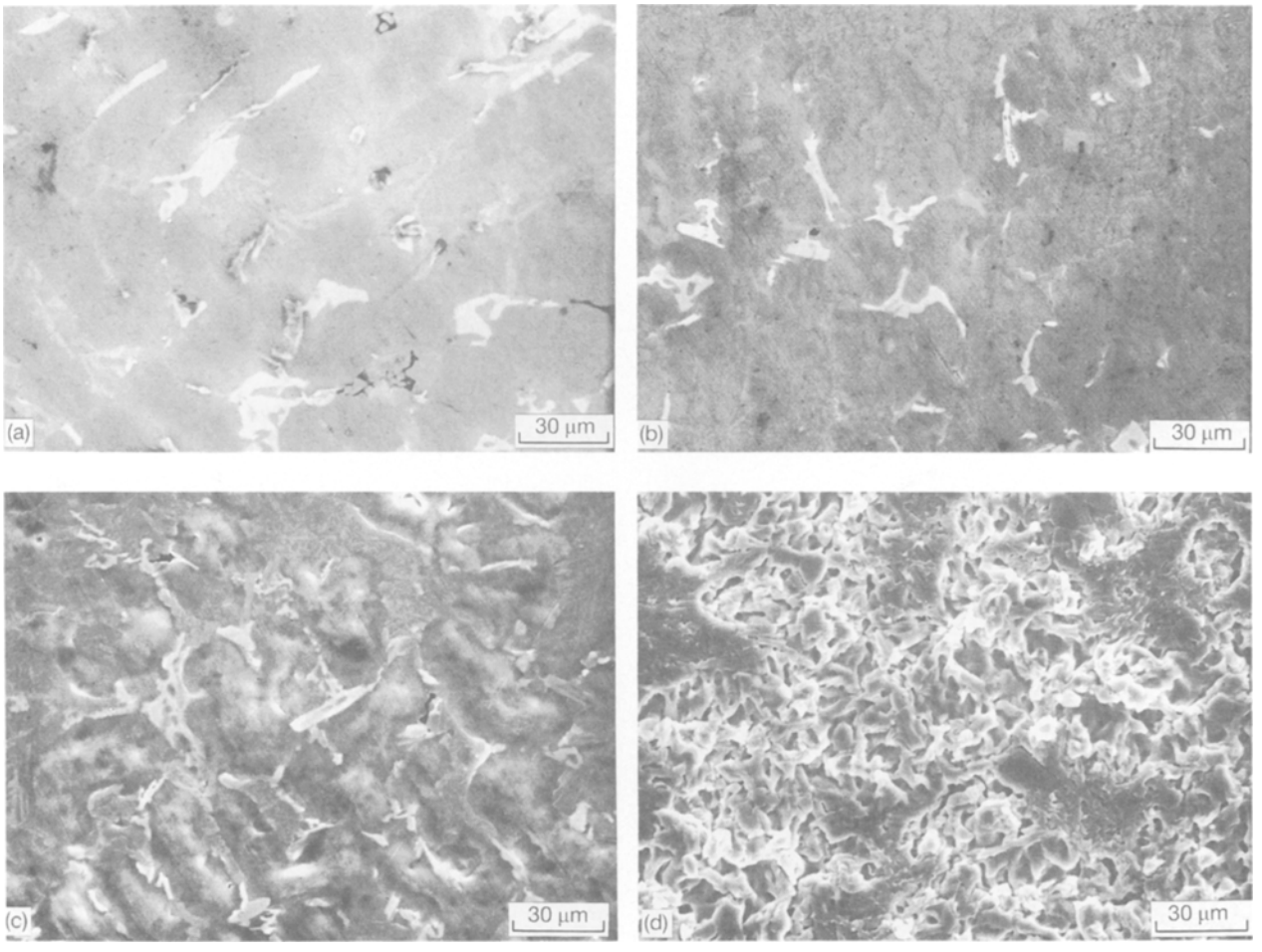

Figure 7 The surface of the Al11Si–AC alloy: (a) polished; and after erosion for (b) 10 s, (c) 1 min, and (d) 10 min.

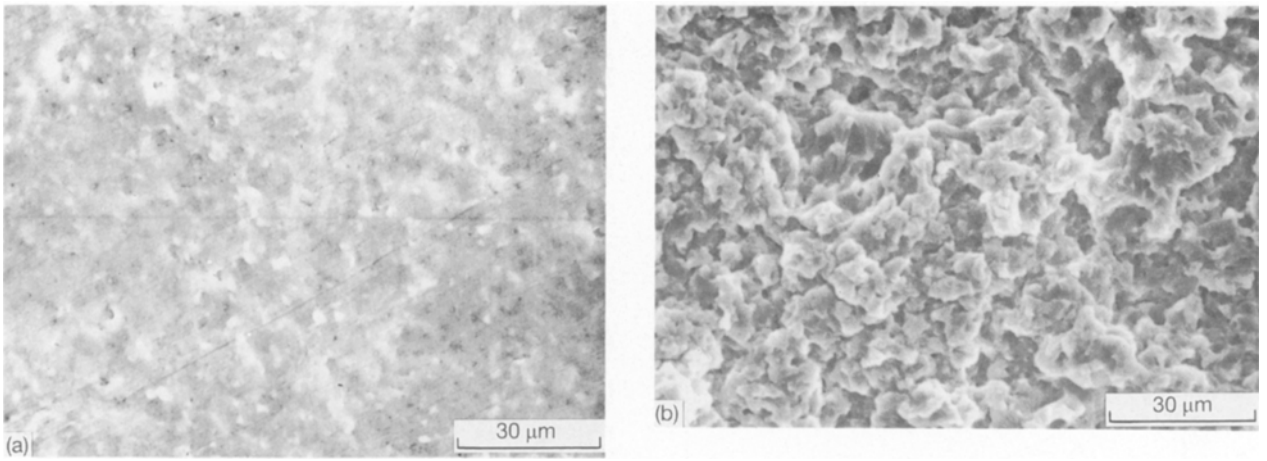

Figure 8 The surface of the AlMgLi–MA alloy after erosion for: (a) 5 min, and (b) 60 min.

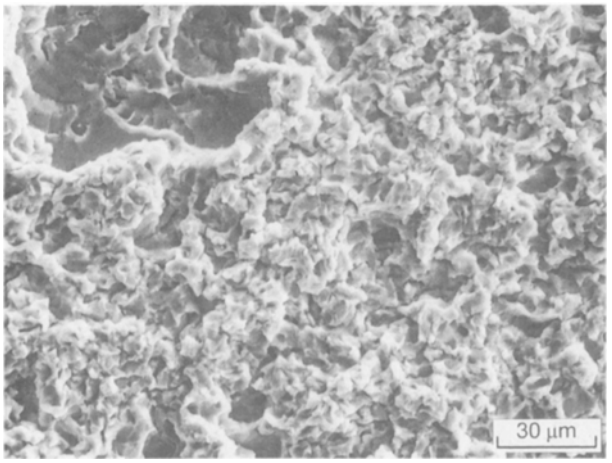

Figure 9 The surface of the AlZn–T7 alloy after erosion for 30 min.

4. Discussion

Cavitation damage generally occurred by plastic deformation of the surface leading to roughening, work hardening, necking, ductile fracture and removal of material. This is consistent with earlier work that cavitation erosion of aluminium was similar to other face-centred-cubic (f.c.c.) metals [6]. However, in the present work, the basic deformation processes are to a large extent modified and controlled by the presence of intermetallic compounds or other microstructural changes, and this is reflected in the considerable variation in the values of the erosion parameters between the different materials.

The Al, AlMg–MA and AlMgLi–MA materials had the simplest microstructures of all the materials. They consisted essentially of fine particles dispersed in a ductile matrix, and deformation was effectively homogeneous and extensive. Consequently, these materials had the longest incubation periods for developing the roughest surfaces. The very fine dispersions of oxide and carbide particles in the mechanically alloyed materials are the basis of a toughness that resisted both the nucleation of pits and loss of material (Fig. 8a), and the continuing loss of material during further deformation. The superior mechanical properties of the AlMgLi–MA alloy compared with those of the AlMg–MA alloy (Table I), is reflected directly in the larger incubation period, lower erosion rate and lower total weight loss of the AlMgLi–MA alloy.

In sharp contrast to the fine and largely uniform microstructures of the above wrought alloys, the cast Al–Si alloys had a coarse network of intermetallic compounds (Figs 4 and 7). The hard compounds concentrated the stress, and localized and limited the flow of the ductile matrix. This promoted the formation of cracks and, to some extent, influenced the crack path (Figs 4 and 7). Thus erosion occurred more readily, and the materials had a low incubation period (Table II) and a low roughness (Table III). The intermetallic compounds are generally undermined and detached from the surface by the removal of the surrounding matrix, but in the Al11Si–AC material, the large volume of the interdendritic microconstituent provided an anchor to the underlying material and the compounds resisted detachment. This left the compounds standing proud of the surface, with the result that the bumpy surface had, most unusually, a positive skewness (Table III). The poor resistances to fracture of the cast structures are also seen in the high erosion rates (Table II). Strengthening the matrix by age-hardening had a dramatic effect on the erosion behaviour of the Al7Si alloy: the incubation period was increased by 200%, the linear rate was decreased by 50% and the total weight loss was reduced by 60%.

Cast aluminium–zinc alloys are inherently strong materials and they are characterized by low erosion rates. A particular feature is the low erosion rate of the cast material compared with the Al–Si cast alloys. The short incubation period also reflects the high strength of the alloys, since only a small amount of deformation will be needed to work harden the surface and to fracture the material.

Hardness is the simplest parameter that has been used to establish, or otherwise, a relation with the erosion rate. The cavitation erosion properties of the present alloys as a function of hardness are shown in Fig. 10. Clearly there were no linear relations between the properties and the hardness. However, the behaviour of the Al–Zn alloys is very significant. On the basis of their incubation period they form a separate and markedly different group (Fig. 10a), whereas, in

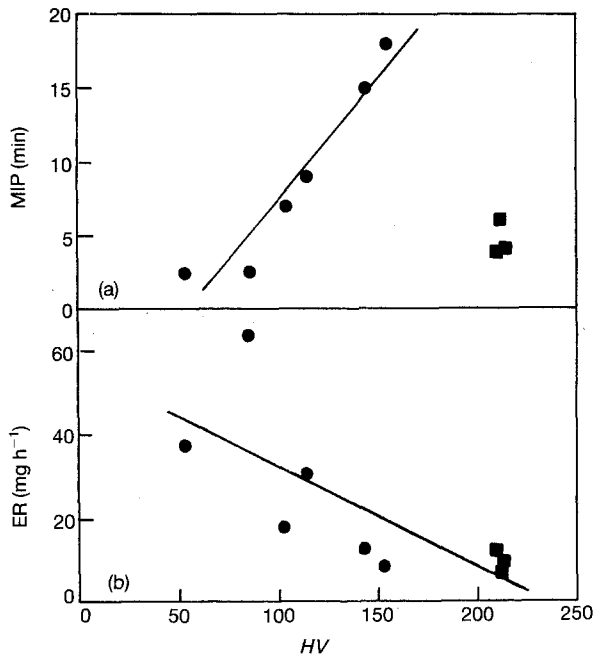

Figure 10 The erosion parameters of all the alloys as a function of the hardness: (a) Measured incubation period (MIP), and (b) erosion rate (ER). (■) Al–Zn alloys, (●) other alloys.

terms of the erosion rate, they show no such distinct behaviour (Fig. 10b). This implies two things. First, the mechanism of accumulation of damage in the incubation period of the Al–Zn alloys is different from that of the other alloys; and secondly, the mechanisms of damage of all the alloys during the period of steady-state erosion is similar. This is reflected in the metallographic aspects of the erosion process.

Despite the considerable variation in the erosion parameters of the materials investigated, there is a similar pattern of deformation and erosion that is modified by the strength and microstructure of the material. Cavitation stresses knead the surface layers and tend to make them flow parallel to the surface. This creates tensile stresses in the surface and cracks tend to form perpendicularly to the surface. Microstructurally homogeneous materials absorb energy by plastically deforming, and this may occur to a considerable extent before work hardening and cracking occur. The presence of intermetallic compounds in the Al–Si alloys limits the amount of deformation and promotes the formation of cracks and the loss of material. Stresses due to cavitation decrease with distance into the surface, and only those layers stressed beyond the yield stress deform. Weak materials readily deform, and ductile fracture occurs. In the stronger Al–Zn alloys, it may be that the slower rate of material removal allows the material just below the yield stress sufficient time to undergo a process of high strain fatigue to produce the removal of patches of material.

5. Conclusions

Under the conditions of cavitation erosion investigated for various aluminium alloys in distilled water the following conclusions can be made.

1. The maximum differences in the incubation period, the linear erosion rate, and the mass loss after 10 h exposure for the different materials were 620%, 740% and 250%, respectively.

2. Mechanically alloyed materials had by far the best combination of erosion-resistant properties. The AlMgLi alloy had the longest incubation period and one of the lowest linear erosion rates.

3. As-cast Al–Si alloys had the shortest incubation period and the highest erosion rates.

4. As-cast Al–Zn alloys had a low incubation period and a low erosion rate.

5. Age hardening the Al7Si alloy increased the incubation period by 300% and decreased the erosion rate by 50%. Age hardening the Al–Zn alloy was far less beneficial.

6. The predominant mechanism of material removal in all alloys was by plastic deformation and ductile fracture. Erosion in the Al–Zn alloys depended on the grain structure, and a fatigue-like process also appeared to be involved in the detachment of material to form flat-bottomed craters.

Acknowledgements

The authors wish to thank A. Jickells of British Gas plc, Gas Research Centre, Loughborough, UK for encouragement and the use of facilities; J. W. Verdon of Milver Metal Co. Ltd., Coventry, for supplying the aluminium–silicon alloys; and A. Brown of Aluminium Service Co., Warwick, UK for supplying the aluminium–zinc alloys.

References

1. A. KARIMI and J. L. MARTIN, *Int. Met. Rev.* **31** (1986) 1.
2. B. VYAS and C. M. PREECE, *J. Appl. Phys.* **47** (1976) 5133.
3. C. J. HEATHCOCK, B. E. PROTHEROE and A. BALL, Proceedings of the 5th International Conference on the Strength of Metals and Alloys, Aachen, August 1979 (Pergamon, Oxford, 1980) Vol. 1, p. 269.
4. R. H. RICHMAN and W. P. McNAUGHTON, *Wear* **140** (1990) 63.
5. B. VYAS and C. M. PREECE, "Cavitation induced deformation of aluminium, erosion, wear, and interfaces with corrosion", ASTM STP 567, (American Society of Testing and Materials, Philadelphia, PA, USA, 1974) pp. 77–105.
6. *Idem., Met. Trans. A* **8** (1977) 915.
7. I. HANSSON and K. A. MØRCH, *J. Phys. D* **11** (1978) 147.
8. P. A. LUSH, R. J. K. WOOD and L. J. CARPANINI, Proceedings of the 6th International Conference on Erosion by Liquid and Solid Impact, Cambridge, September 1983 (Cavendish Laboratory, Cambridge University, Cambridge, 1983) pp. 5-1/5–8.
9. S. VAIDYA and C. M. PREECE, *Met. Trans. A* **9** (1978) 299.
10. B. C. S. RAO and D. H. BUCKLEY, Proceedings of the 6th International Conference on Erosion by Liquid and Solid Impact, Cambridge, September 1983 (Cavendish Laboratory, Cambridge University, Cambridge, 1983) pp. 8–1/8–5.
11. B. C. S. RAO and D. H. BUCKLEY, *Mater. Sci. Engng.* **67** (1984) 55.
12. *Idem., Wear* **105** (1985) 171.
13. K. J. SAWLEY, *Metals Mater.* **5** (1989) 210.
14. S. J. MATTHEWS, PhD thesis, Coventry University, Coventry, UK, (1993).
15. K. STOUT, *Mater. Engng.* **2** (1981) 260.

Received 7 June 1993
and accepted 26 August 1993